JOURNAL OF OPTOELECTRONICS AND ADVANCED MATERIALS Vol. 8, No. 5, October 2006, p. 1660 - 1666

Invited Paper

Analysis of magnetic transitions through the magnetoimpedance effect

C. GÓMEZ-POLO*, V. RECARTE, J. I. PÉREZ-LANDAZABAL
Departamento de Física. Universidad Pública de Navarra. Campus de Arrosadia 31006 Pamplona. Spain

The temperature dependence of the magnetoimpedance effect represents a powerful research tool in the analysis of those magnetic transitions associated with changes in the magnetic permeability of the system. Both, in the low frequency region (magnetoinductance effect) and in the higher frequency regime where the skin effect takes place, the AC complex impedance, *Z*, is mainly determined by the transverse magnetic permeability. Thus, its temperature dependence and its evolution under applied external magnetic field, *Z(T, H),* are directly correlated with the temperature dependence of the basic magnetic parameters, in particular, the magnetic permeability of the system. In this work, this AC magnetotransport effect has been employed to analyse the characteristic transition in two magnetic systems: (i) the magnetic transition in Fe based soft magnetic nanocrystalline alloys associated with the decoupling of the ferromagnetic crystallites around the Curie point of the residual amorphous phase; (ii) the martensitic transformation in ferromagnetic shape memory alloys (NiMnGa), from a highly anisotropic martensite phase to the austenite phase. The results indicate the suitability of this simple AC magnetotransport technique to analyse the main features of the characteristic magnetic transition of these systems.

(Received September 5, 2006; accepted September 13, 2006)

Keywords: Magnetic transitions, Magnetoimpedance effect, Soft magnetic nanocrystalline alloys, Ferromagnetic shape memory alloys

1. Introduction

The magnetotransport properties of new nanostructured materials represent a research topic of continuous growing interest from both basic and applied points of view [1]. Among them, the so-called Giant Magnetoimpedance effect stands out: the occurrence of huge variations of the electrical impedance of a soft magnetic material under the application of an external magnetic field [2].

When an AC current flows through a ferromagnetic conductor, the associated transverse magnetic field magnetizes the sample. For high enough current frequencies, *f,* the current flows in a reduced region closed to the sample surface (*skin effect*). Within the classical electrodynamical theory, the complex impedance *Z* can be expressed for different sample geometries [3]:

$$Z = \frac{1}{2} R_{dc} ka \frac{J_o(ka)}{J_1(ka)} \quad (wire) \qquad (1.a)$$

$$Z = R_{dc} kz coth(kz) \quad (ribbon) \qquad (1.b)$$

with $k = \sqrt{\frac{i2\pi f\mu_\phi}{\rho}}$, μ_ϕ the circular or transverse permeability, ρ the electrical resistivity, *a* the wire radius, *z* the ribbon thickness, R_{dc} the ohmic resistance, J_i the Bessel functions of first kind.

Thus, the complex impedance turns out to be mainly governed by the transverse magnetization process under the magnetizing field generated by the flow of the electrical current. The application of an external axial DC field generates a hard axis with respect to the transverse direction, leading to sensitive changes in μ_ϕ in soft magnetic samples, and accordingly, to huge variations in *Z*.

From a technological point of view, its main interest lies in the design of highly sensitive micromagnetic sensors [4]. However, the effect can also be employed as a research tool in the analysis of the basic characteristics of the samples, i.e. study of the intrinsic magnetoelastic anisotropies in amorphous wires [5] and nonlinear characteristics of the effect (occurrence of higher harmonics in the magnetoimpedance voltage) [6].

On the other hand, the magnetic permeability in nanostructured materials is strongly determined by thermal effects. Accordingly, the AC complex impedance, and in particular, the GMI effect can be employed to magnetically characterize those magnetic transitions where the magnetic permeability of the system displays remarkable variations. In this sense, the main aim of the work is to show the suitability of this AC magnetostransport effect to analyse the characteristic magnetic transition in two magnetic systems: (i) the magnetic transition in Fe based soft magnetic nanocrystalline alloys associated with the decoupling between the ferromagnetic crystallites around the Curie point of the residual amorphous phase; (ii) the martensitic transformation in ferromagnetic shape memory alloys, from the low temperature highly anisotropic martensitic phase to the high temperature austenic phase. The results clearly indicate the suitability of this simple AC magnetostransport technique to analyse the characteristic magnetic transition of these systems. This characterization

technique displays optimized features with respect to the conventional induction determination of the AC magnetic permeability, basically in terms of its simplicity (four-point technique measuring configuration, avoiding the use of excitation and pick-up coils) and high sensitivity. However, some disadvantages should also be outlined correlated with the particular sample requirements. The transverse magnetic field generated by the flow of the electrical current should be able to transversally magnetize the sample. Therefore, maximum sensitivities of this AC characterization technique are achieved in high permeability soft magnetic samples (high μ_ϕ values), with reduced transverse dimensions (high current densities) and circular cross section (wires) (reduction of the demagnetizing effects along the transverse direction).

2. Experimental techniques

Amorphous wires (diameter 120 μm) with nominal composition $Fe_{66.5}Cr_7Si_{13.5}B_9Cu_1Nb_3$ and $Fe_{73.5}Si_{13.5}B_9Cu_1Nb_3$ were obtained from rapid quenching from the melt (in-rotating-water-quenching technique). In order to promote the characteristic nanocrystalline state, the alloys were isothermally annealed in vacuum at their corresponding crystallization temperatures. In the case of the ferromagnetic shape memory alloys, policrystalline ribbons with nominal composition $Ni_{52.5}Mn_{24.5}Ga_{23}$ (10 mm, 50 μm thick) were obtained by melt-spinning technique.

Magnetoimpedance measurements (77 K – 300 K; 350 K – 550 K; driving frequencies, *f*, 1 – 100 kHz) were performed under a conventional four-point technique, using a commercial *LCR* meter (STANFORD SR720) and a home-made impedance analyser using a lock-in amplifier (sample lengths ≈ 5 cm). Both experimental set-ups allowed the characterization of the temperature dependence of the complex AC electrical impedance, *Z*, under the action of an axial DC magnetic field generated by a long solenoid. For comparison, the axial AC magnetic susceptibility was simultaneously determined through a conventional induction method.

3. Results and discussion

3.1. Fe-based nanocrystalline wires

The soft magnetic behavior of Fe-rich nanocrystalline alloys has been extensively studied during the last decade [7, 8]. Their excellent soft magnetic response is directly correlated to their ultrafine structure composed of bcc-Fe rich crystals (nanometer size) surrounded by a residual amorphous matrix. This magnetic softening is mainly ascribed to the averaging out of the magnetocrystalline anisotropy via the magnetic interactions between the two constituent magnetic phases and is reinforced by the negligible magnetoelastic contribution due to the reduction of both, the internal quenched stresses and the effective magnetostriction.

Within the framework of the random anisotropy model, the effective magnetocrystalline anisotropy, k_{eff}, is mainly expressed in terms of the structural and magnetic characteristics of the precipitated crystalline phase (v_C: crystalline fraction; *d*: mean grain size; k_1: magnetocrystalline anisotropy [9]:

$$k_{eff} = \frac{v_C^{\,2} k_1^{\,4} d^6}{A^3} \qquad (2)$$

where $A = \sqrt{A_1 A_2}$ represents the mean exchange constant of the coupled system (A_1 and A_2 the exchange constants of the crystalline and amorphous phases, respectively). Thus, the role of the residual amorphous phase cannot be disregarded and its exchange transmission capacity mainly determines the macroscopic magnetic response, especially around the Curie point of the residual amorphous phase (T_{C2}) [10]. So, a magnetic transition takes place around this Curie point, associated with the magnetic decoupling between the ferromagnetic crystallites with higher Curie point. Such a magnetic transition is experimentally detected as a sharp increase and decrease, respectively, of the coercivity [11] and magnetic permeability [12] around T_{C2}.

The crystallization process of the initial amorphous FeSiBCuNb alloys mainly consists of two well defined processes at T_{x1} and T_{x2}, ascribed to the precipitation of bcc-FeSi and boride phases, respectively [13]. Thus, the desired nanocrystalline structure in these soft magnetic nanocrystalline alloys is achieved by submitting the initial amorphous structure to suitable isothermal annealings at temperatures $T_a \approx T_{x1}$. In the particular case of the analyzed FeCrSiBNb system, previous structural studies (Differential Scanning Calorimetry, DSC, and Neutron Diffractometry) [14, 15, 16] indicate that the crystallization processes of the alloys are not basically modified with the inclusion of Cr atoms (a slight increase in both T_{x1} and T_{x2} with the Cr content of the alloy). Upon crystallization of the bcc-FeSi phase the enrichment of Cr atoms of the residual amorphous phase promotes a sharp decrease of the Curie point of the residual amorphous phase [15]. According to the performed magnetic characterization (temperature dependence of the saturation magnetization and AC axial magnetic permeability), the residual amorphous phase of the nanocrystalline $Fe_{66.5}Cr_7Si_{13.5}B_9Cu_1Nb_3$ alloy (T_a = 597°C during 10 min) is characterized by a Curie temperature T_{C2} = 160 K.

Fig. 1a displays the temperature dependence of the complex impedance $Z = R + iX$ (*R*: resistance; $X = 2\pi fL$; *L*: inductance) for exciting frequency *f* = 100 kHz and exciting voltages V_{ac} = 0.1 and 1 V (LCR meter). As expected, the magnetic transition associated with the magnetic decoupling process of the ferromagnetic crystallites around T_{C2} can be clearly detected by a sharp decrease in the impedance components for V_{ac} = 1 V. For $T < T_{C2}$ the characteristic soft magnetic response of the nanocrystalline system promotes a strong skin effect in the sample, giving rise to maximum values in *Z*. For $T > T_{C2}$ the sample magnetically behaves as a set of single domain ferromagnetic particles (superparamagnetic behaviour [17]), with reduced magnetic permeabilty and neglegible skin effect. However, the lower exciting voltage (V_{ac} = 0.1 V), that is, the lower amplitude of the exciting current,

gives rise to a temperature dependence of the resistive component similar to the non magnetic ohmic resistance $R_{dc}(T)$. Under these experimental conditions, the associated circumferential magnetic field generated by the flow of the electrical current, is not able to magnetize the sample (low μ_ϕ values). In fact, for low k values ($k = \sqrt{\frac{i2\pi f\mu_\phi}{\rho}}$), the complex impedance (eqs. 1) can be expressed as (*magnetoinductive effect*):

$$Z = R_{dc} + i\frac{< E_Z >}{I}L \qquad (3)$$

where $< E_z >$ represents the average electrical field originated by the circumferential magnetization process ($< E_z > \propto \mu_\phi$). Thus, low frequency values should promote a similar behaviour, that is, $R(T) \approx R_{dc}(T)$ and $X(T) = 2\pi fL(T) \propto \mu_\phi(T)$ (see Fig. 1b, where the temperature dependence of the complex impedance is plotted for f = 1 kHz).

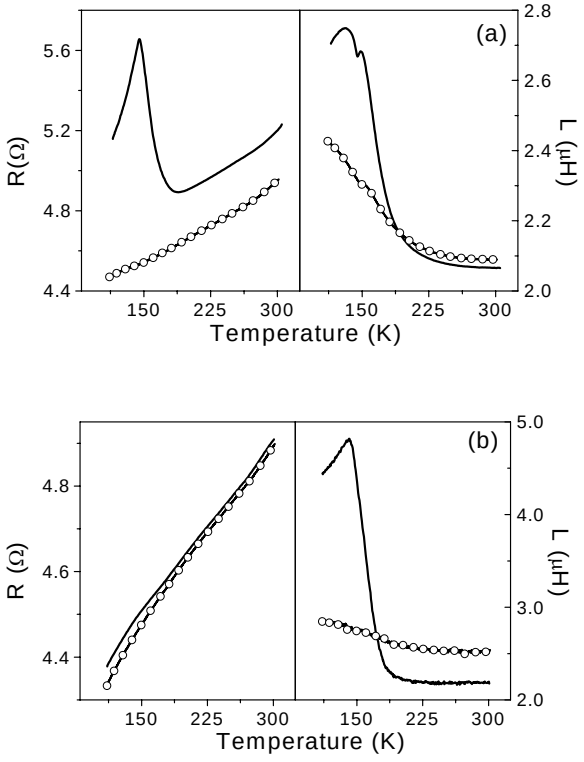

Fig. 1. Temperature dependence of the resistance (R) and inductance (L) for (○) V_{ac} = 1 V and (–) V_{ac} = 0.1 V at (a) f = 100 kHz and (b) f = 1 kHz for the $Fe_{66.5}Cr_7Si_{13.5}B_9Cu_1Nb_3$ nanocrystalline wire.

With respect to the axial field (H) dependence of Z (GMI effect), Figs. 2 and 3, displays $R(H)$ and $L(H)$ for f = 100 and 1 kHz, respectively (V_{ac} = 1 V), at some selected measuring temperatures. In the high frequency region (f = 100 kHz, see Fig. 2) for $T < T_{C2}$, where the skin effect dominates the impedance response, the application of the axial magnetic field promotes remarkable variations in both resistive and inductive components as a consequence of the parallel changes in μ_ϕ with H. The decrease in the exciting frequency (f = 1 kHz, see fig. 3) leads according to eq. 3, to negligible field variations in R. However, L displays in this low frequency region, the characteristic axial field dependence of μ_ϕ, that is, hysteretic behaviour and the occurrence of a maximum value for applied fields, $H \approx \pm H_K = \frac{2k_{eff}}{\mu_0 M_S}$ (H_K: mean circumferential anisotropy field; M_S: saturation magnetization) [18]. Thus, the position of this maximum can be employed to analyze the characteristic decoupling process of the ferromagnetic crystallites around T_{C2}. As the inset of Fig. 4 shows, the maximum in L shifts towards higher H values as T increases. This increase in H_K should be interpreted as a consequence of the parallel increase in the effective magnetocrystalline anisotropy of the system as T approaches T_{C2}. Such an increase is displayed in Fig. 4, where the mean value of anisotropy field is plotted as a function of the measuring temperature. As expected, the decopling process for $T > T_{C2}$ promotes a sharp increase in H_K.

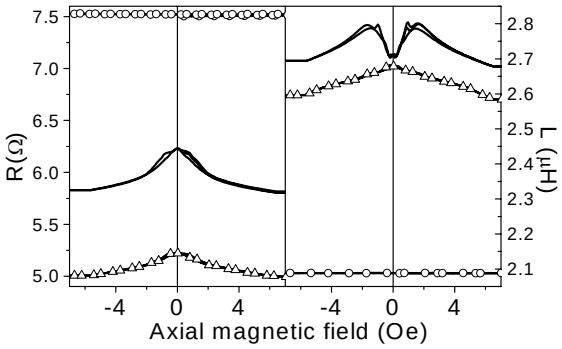

Fig. 2. Axial field dependence of the resistance (R) and inductance (L) at f = 100 kHz and V_{ac} = 1 V for the $Fe_{66.5}Cr_7Si_{13.5}B_9Cu_1Nb_3$ nanocrystalline wire: (○) T = 110 K, (Δ) T = 140 K and (–) T = 300 K.

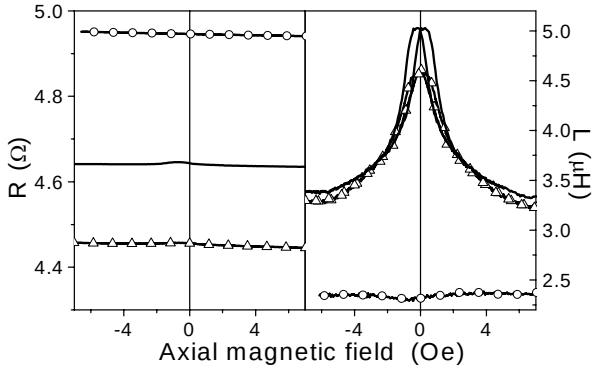

Fig. 3. Axial field dependence of the resistance (R) and inductance (L) at f = 1 kHz and V_{ac} = 1 V for the $Fe_{66.5}Cr_7Si_{13.5}B_9Cu_1Nb_3$ nanocrystalline wire: (○) T = 113 K, (Δ) T = 148 K and (–) T = 200 K.

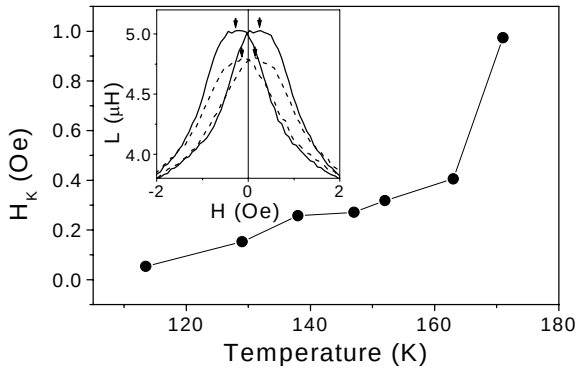

Fig. 4. Temperature dependence of the anisotropy field, H_K for the $Fe_{66.5}Cr_7Si_{13.5}B_9Cu_1Nb_3$ nanocrystalline wire. Inset: Axial field dependence of the inductance (L) at f = 1 kHz and V_{ac} = 1 V:(_ _ _) T = 129 K,(_) T =148 K.

This simple and highly sensitive technique, in particular, the temperature dependence of Z, can be also employed in the analysis of some other features of the characteristic decoupling process in these soft magnetic nanocrystalline alloys. When this magnetic transition is analyzed through AC inductive techniques (i.e. the temperature dependence of the AC axial magnetic permeability) it is found a strong dependence of the associated transition temperature with the amplitude of applied magnetic field [15, 19]. As an example, Fig. 5 shows the temperature dependence of the complex AC magnetic susceptibility, $\chi = \chi_r + i\chi_i$, for different values of the amplitude of the exciting axial AC magnetic field, H_{ac}, (f = 500 Hz). The displayed $\chi(T)$ corresponds to a $Fe_{73.5}Si_{13.5}B_9Cu_1Nb_3$ wire, annealed at T_a = 550 °C during 30 min. The obtained nanocrystalline structure is characterized by a 80% of bcc-FeSi nanocrystals (12 nm in size) surrounded by the residual amorphous phase with T_{C2} ≈ 340°C. As fig. 5 shows, the temperature dependence of the real (χ_r) and imaginary (χ_i) susceptibility components are characterized by a sharp decrease and a maximum value, respectively, around $T \approx T_{C2}$ (magnetic decoupling between ferromagnetic crystallites). Surprisingly, the magnetic transition shifts towards higher temperatures with the amplitude of the AC magnetic field.

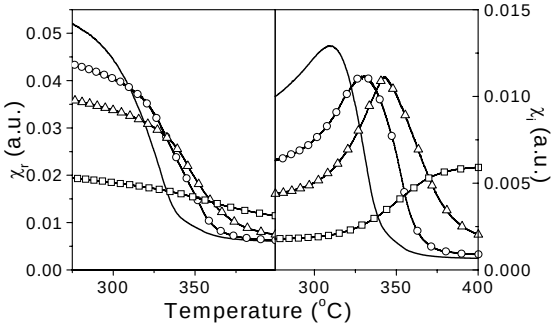

Fig. 5. Magnetic susceptibility, $\chi = \chi_r + i\chi_i$, versus temperature for different values of the amplitude of the AC magnetic field, H_{ac} ((□) 38 A/m, (–) 76 A/m, (○) 114 A/m, (Δ) 304 A/m) in the $Fe_{73.5}Si_{13.5}B_9Cu_1Nb_3$ nanocrystalline wire.

Since the complex electrical impedance is mainly governed by the transverse magnetization process, a similar effect should be detected in the temperature dependence of Z. Fig. 6a and 6b show, respectively, the resistance, R, and reactance, X, as a function of the measuring temperature for f = 100 kHz and 1 kHz and amplitudes of the electrical current, I_{ac}, 5 and 20 mA. As previously discussed (see Fig. 1), the increase in the exciting frequency, f, gives rise to a remarkable increase in both impedance components. As expected, a clear shift of the magnetic transition (sharp decrease in both impedance components for $T \approx T_{C2}$) is experimentally detected with the increase in I_{ac}. This behaviour is a direct consequence of the dependence of $\mu_\phi(T)$ on the mean circumferential magnetic field ($H_\phi \propto I_{ac}$) acting on the sample.

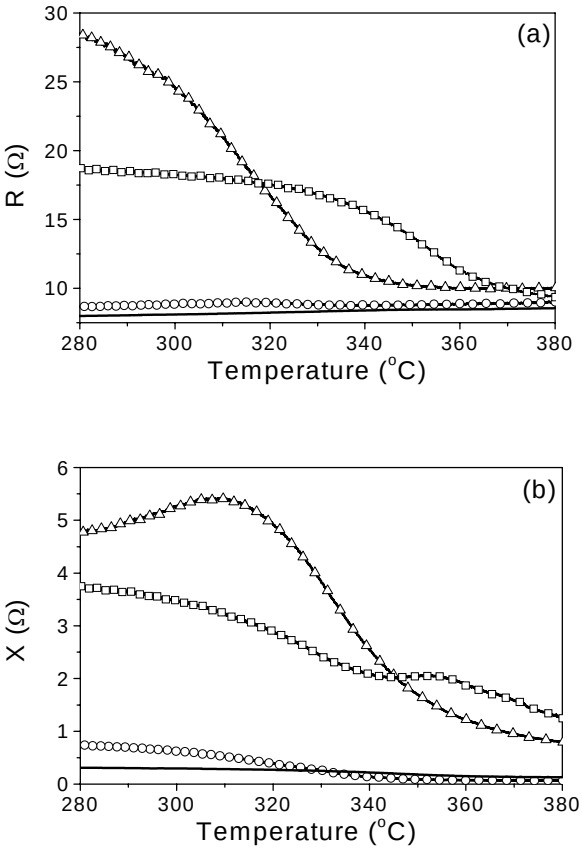

Fig. 6. Temperature dependence of (a) the resistance (R) and (b) reactance (X) for f = 1 kHz ((–) I_{ac} = 5 mA and (□) I_{ac} = 20 mA) and f = 100 kHz ((○) I_{ac} = 5 mA and (Δ) I_{ac} = 20 mA) for the $Fe_{73.5}Si_{13.5}B_9Cu_1Nb_3$ nanocrystalline wire.

For comparison, Fig. 7 displays the temperature dependence of the magnetic loss factor defined for (a) the magnetic susceptibility, $tg\ \delta = \chi_i / \chi_r$, and (b) for the electrical impedance, $tg\ \delta = R/X$, at different values of the amplitude of axial magnetic field (H_{ac}) and electrical current (I_{ac}), respectively. In both cases, a maximum value in $tg\ \delta$ is experimentally detected around

T_{C2} that should be ascribed to the enhancement in the irreversible contribution associated with the magnetic decoupling between the ferromagnetic crystallites. Notice the shift of the maximum towards higher measuring temperatures with the amplitude of the exciting AC magnetic field acting on the sample (axially or circumferentially, for χ and Z, respectively).

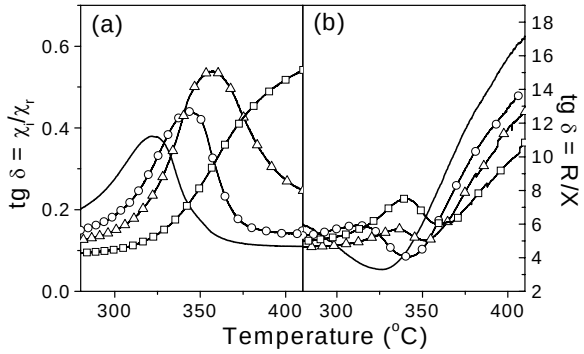

Fig. 7. Magnetic loss factor as a function of temperature for the $Fe_{73.5}Si_{13.5}B_9Cu_1Nb_3$ nanocrystalline wire: (a) $tg\ \delta = \chi_i/\chi_r$ and H_{ac} = (□) 38 A/m, (–) 76 A/m, (○) 114 A/m, (Δ) 304 A/m; (b) $tg\ \delta = R/X$ and I_{ac} = (□) 5 mA, (–) 10 mA, (○) 15 mA, (Δ) 20 mA.

The detected field dependence can be well understood in terms of the AC nature of both magnetic characterizations (AC axial magnetic susceptibility and complex electrical impedance). It should be kept in mind that such AC characterizations imply the excitation with a sinusoidal mean magnetic field of amplitude H_{ac}. It can be demonstrated the direct relationship between the transition temperature, T_P, (measuring temperature where $tg\ \delta$ reaches a maximum value) and the measuring temperature where the amplitude of the AC magnetic, H_{ac}, field equals the sample coercivity, H_C [19]. The increase of T_P with H_{ac} (or I_{ac}) should be interpreted as a result of the characteristic increase of H_C of these nanocrystalline systems associated with the magnetic decoupling process of the ferromagnetic crystallites around T_{C2}. Starting at low T, consider a value of H_{ac} higher than H_C ($H_{ac} > H_C$). As T increases, the progressive magnetic hardening around T_{C2} promotes a parallel decrease and increase, respectively, in the real and imaginary component of the magnetic susceptibility (increase in H_C). At a certain measuring temperature, H_{ac} equals H_C. A further increase of T above this critical point leads to a parallel decrease in both susceptibility components since the applied magnetic field is not able to magnetize the assembly of ferromagnetic particles ($H_{ac} < H_C$). Therefore, as H_{ac} increases, the condition $H_{ac} = H_C$ is fulfilled at higher temperatures, giving rise to detected field dependence *tg δ(T)*. Thus, the detected temperature dependence of both susceptibility components can be easily explained in terms of relationship between H_{ac} and $H_C(T)$, that is, a continuous decrease of the real component around T_{C2} and a maximum value in imaginary contribution at the measuring temperature where $H_{ac} = H_{C.}$

Accordingly, the shift of the temperature dependence of Z with the amplitude of the exciting current, I_{ac}, should be interpreted in a similar way. In the high frequency region (f = 100 kHz) where the skin effect takes place, both impedance components drastically decrease at the measuring temperatures where the mean amplitude of H_ϕ equals the circumferential coercivity of the sample, $H_{C,\phi}$. Above this critical temperature, the mean circumferential field is not able to magnetize the single domain magnetic system, leading to the sharp decrease in the mean value of μ_ϕ and thus to the dissappearance of the skin effect of the sample. Again, as I_{ac} increases, the condition $H_\phi = H_{C,\phi}$ is fulfilled at higher temperatures, leading to the detected field dependence of *Z(T)*.

3.2. Ferromagnetic shape memory alloys

The main characteristic of the Ferromagnetic Shape Memory alloys (FSM) is the occurrence of a martensitic transformation (first-order diffusionless phase transition) from a high-temperature low anisotropy austenitic phase to a low-temperature closed packed martensitic phase [20]. The high magnetocrystalline anisotropy of the low-temperature martensitic phase promotes in these FSM alloys remarkable magnetostrictive properties. In particular, magnetic-field-induced strains around 6 % have been experimentally detected in Ni_2MnGa single crystals [21]. The twin boundary motion in the martensite rearranges the variant structure to minimize the elastic and magnetic stored energies, giving rise to the macroscopic shape change [22]. From a technological point of view, the main interest of these alloys is related with the design of new magnetic actuators (i.e. linear motors).

The characteristic martensitic transformation promotes strong modifications in the basic electrical and magnetic parameters of the alloy. In particular, a sharp decrease and increase in the electrical resistivity, ρ, and magnetic permeability, μ, respectively, from the low temperature martensitic to the high temperature austenic phase [23, 24]. Thus, since the complex impedance, Z, is mainly governed by $k = \sqrt{\dfrac{i2\pi f\mu_\phi}{\rho}}$, the martensitic transformation should give rise to strong modifications in the skin effect and thus to a remarkable increase in both impedance components.

Fig. 8 shows the temperature dependence of both impedance components of the melt-spun $Ni_{52.5}Mn_{24.5}Ga_{23}$ ribbon, at exciting frequency f = 100 kHz and I_{ac} = 30 mA. The resistive component (R) displays the characteristic temperature dependence of the ohmic resistance of these FSM alloys, that is, a sharp decrease associated with the martensite (low temperature) to austenite (high temperature) transformation. Moreover, the occurrence of the characteristic thermal hysteresis upon heating and cooling is also experimentally detected. The Curie point of the austenitic phase can be clearly seen as a change in the slope of *R(T)*. With respect to the temperature dependence

of imaginary component, *X(T)* directly reflects the temperature dependence of the magnetic permeability [25]: a sharp increase associated with the martensitie-to-austenite transformation followed by a progressive diminution around the Curie point of the austenite phase. The occurrence of thermal hysteresis associated with the martensitic transformation is also experimentally detected in *X(T)*.

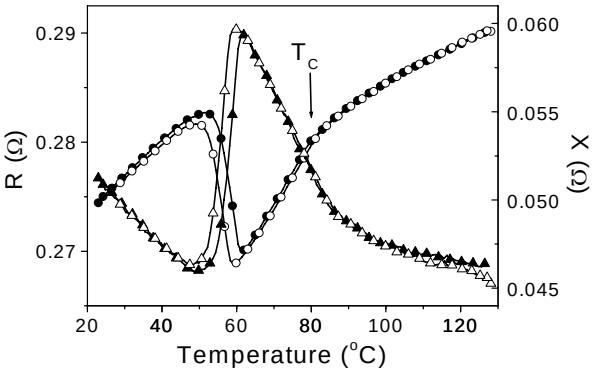

Fig. 8. Temperature dependence of the impedance components, resistance (R) ((▲) heating (Δ) cooling) and reactance (X) ((○) heating (•) cooling) for f = 100 kHz and I_{ac} = 30 mA: in the melt-spun $Ni_{52.5}Mn_{24.5}Ga_{23}$ ribbon.

The obtained temperature dependence of both impedance components, that is, $R(T) \approx R_{dc}(T)$ and $X(T)) \propto \mu(T)$, indicates the absence of skin effect (low *k* values, *magnetoinductive effect*) under the employed experimental conditions (*f* = 100 kHz and I_{ac} = 30 mA). In order to enhance the skin effect (increase in *k*) and thus to promote remarkable changes in both impedance components around the characteristic martensitic transformation, the effect of exciting frequency (*f* from 100 to 1 MHz) and amplitude of the exciting current (I_{ac} from 5 to 65 mA) were analyzed. The results show that the low permeability values of these FSM alloys basically determine their impedance behaviour (i.e. negligible skin effect). While *R(T)* does not display remarkable changes with *f* and I_{ac}, a noticeable decrease in *X(T)* with *f* is experimentally detected as a consequence of the magnetic relaxation of the sample (decrease of μ with *f*).

4. Conclusions

The temperature dependence of the magneto-impedance (MI) effect represents a powerful research tool in the analysis of those magnetic transitions associated with changes in the magnetic permeability of the magnetic system. The temperature dependence of the complex impedance, *Z*, and its evolution under applied external magnetic field, *Z(T, H),* are directly correlated with the temperature dependence of the basic magnetic parameters, in particular, the magnetic permeability of the system.

In the case of the Fe-based soft magnetic nanocrystalline alloys, the MI effect can be suitably employed to analyze the characteristic magnetic transition associated with the decoupling between the ferromagnetic crystallites around the Curie point of the residual amorphous phase, T_{C2}: (i) a sharp decrease in both impedance components at $T \approx T_{C2}$; (ii) the occurrence of maximum MI ratios (maximum axial field dependence of *Z*) at $T \approx T_{C2}$; (iii) An increase in the mean anisotropy field with the magnetic decoupling between the ferromagnetic crystallites; (iv) the field dependence of the magnetic losses around T_{C2}.

On the other hand, in spite of the low magnetic permeability of the ferromagnetic shape memory alloys (NiMnGa), the temperature dependence of the complex impedance reflects the basic features of the characteristic martensitic transformation. In this case, although the skin effect is negligible, this simple AC magnetometry technique allows the simultaneous characterization of temperature dependence of the electrical resistivity and magnetic permeability at the martesitic transformation.

As a final conclusion, it should be outlined that the results obtained in two different magnetic systems (soft magnetic nanocrystalline and ferromagnetic memory shape alloys) indicate the suitability of this simple AC magnetotransport technique to analyse the main features of different magnetic transitions.

Acknowledgments

The authors wish to thank the following collaborators that have deeply contributed to the work: Prof. M. Vázquez , Prof. A. Hernando and Prof. E. Cesari. The work was supported by the Spanish "Ministerio de Ciencia y Tecnología" (projects MAT-1999-0422-C02 and MAT2003-05243) and the "Gobierno de Navarra" (project "Propiedades de magnetotransporte de nuevos materials nanoestructurados).

References

[1] M. Knobel, J. C. Denardin, A. L. Brand, Materials Science Forum **403,** 117 (2002).
[2] M. Knobel, L. Kraus, M. Vázquez, "Giant Magnetoimpedance", in Handbook of Magnetism and Magnetic Materials, vol. 12, Ed. K. H. J. Buschow (Elsevier, New York, 2003) 497.
[3] L. D. Landau, E. M. Lifschitz, L. P. Pitaevski, Electrodynamics of Continuous Media (Buttherworth-Heinemann, London, 1995) p. 212.
[4] K. Mohri, T. Uchiyama, L. P. Shen, C. M. Cai, L. V. Panina, J. Magn. Magn. Mat., **249,** 351 (2002).
[5] I. Betancourt, R. Valenzuela, Appl. Phys. Lett. **83,** 2022 (2003).
[6] C. Gómez-Polo, J.G.S. Duque, M. Knobel, J. Phys.: Condens. Matter **16,** 5083 (2004).
[7] G. Herzer, "Nanocrystalline soft magnetic alloys", in Handbook of Magnetic Materials, Ed. KH.J. Buschow (Elsevier, Amsterdamm, 1997), vol. 10, p. 415.

[8] K. Hono, M. Ohuma, in Magnetic Nanostructures (American Scientific Publishers, California, 2002), chapter 8, p. 366.
[9] J. Arcas, A. Hernando, J.M. Barandiarán, C. Prados, M. Vázquez, P. Marín, A. Neuweiler, Phys. Rev. B, **58,** 5193 (1998).
[10] K. Suzuki, J.M. Cadogan, Phys. Rev. B, **58**, 2730 (1998).
[11] A. Hernando, P. Marín, M. Vázquez, J. M. Barandiarán, G. Herzer, Phys. Rev. B, **58,** 366 (1998).
[12] C. Gómez-Polo, J. I. Pérez-Landazabal, V. Recarte, J. Campo, P. Marín, M. López, A. Hernando, M. Vázquez, Phys. Rev. B, **66,** 012401 (2002).
[13] F. Zhu, N. Wang, R. Busch, P. Haasen, Script. Metall. et. Mater., **25,** 2011 (1991).
[14] C. Gómez-Polo, Y.F. Li, J. I. Pérez-Landazabal, V. Recarte, M. Vázquez, Sensors & Actuators A, **106,** 230 (2003).
[15] C. Gómez-Polo, J. I. Pérez-Landazabal, V. Recarte, IEEE Trans. Magn., **39**, 3019 (2003).
[16] V. Recarte, J. I. Pérez-Landazabal, C. Gómez-Polo, Physica B: Cond. Matt., **350**, E135 (2004).
[17] V. Franco, L.F. Kiss, T. Kemény, I. Vinze, C. F. Conde, A. Conde, Phys. Rev. B, **66,** 224418 (2002).
[18] C. Gómez-Polo, M. Vázquez, J. Magn. Magn. Mat., **272-276**, 357, (2004).
[19] C. Gómez-Polo, J. I. Pérez-Landazabal, V. Recarte, M. Vázquez, A. Hernando, Phys. Rev. B, **70**, 094412 (2004).
[20] "Science and technology of shape-memory alloys: new developments" in *MRS Bulletin*, Eds. K. Otsuka and T. Kakeshita (2002) vol. 27.
[21] K. Ullako, J. K. Huang, V. V. Kokorin, R. C. O´Handley, Appl. Phys. Lett. **69,** 1133, (1996).
[22] R. C. O´Handley, S. J. Murray, M. Marioni, H. Nembach, S. M. Allen, J. Appl. Phys. **87**, 4712 (2000).
[23] X. Jin, D. Bono, R. C. O'Handley, S. M. Allen, T. Y. Hsu, J. Appl. Phys. **93,** 8630 (2003).
[24] O. Heczko, N. Lanska, O. Soderberg, K. Ullakko, J. Magn. Magn. Mat., **242-245,** 1446 (2002).
[25] J. I. Pérez-Landazabal, C. Gómez-Polo, V. Recarte, C. Seguí, E. Cesari, P. Ochin, J. Magn. Magn. Mat., **290-291**, 826 (2005).

*Corresponding author: gpolo@si.unavarra.es